Desalination and Water Treatment
www.deswater.com

doi: 10.5004/dwt.2022.28594

265 (2022) 57–70
July

Effective Cu(II) ions adsorption from aqueous solutions using low grade oolitic hematite tailing with phosphorus: response surface methodology

Xiaoli Yuan*, Fuming Luo, Xixi Chen, Wentang Xia*, Yin Zou, Xuejiao Zhou, Hao Liu, Youjie Song, Jie He, Shengzhi Ma

School of Metallurgy and Material Engineering, Chongqing University of Science and Technology, Chongqing 401331, China, Tel./Fax: +862365023436; emails: yuanxiaoli1981@126.com (X. Yuan), wentangx@163.com (W. Xia), 1658325145@qq.com (F. Luo), 791927060@qq.com (X. Chen), 2455843935@qq.com (Y. Zou), zxj040203017@126.com (X. Zhou), liuhao_023@163.com (H. Liu), 1547168269@qq.com (Y. Song), 2649600403@qq.com (J. He), 1257902115@qq.com (S. Ma)

Received 13 December 2021; Accepted 19 May 2022

ABSTRACT

In this work, low grade oolitic hematite tailing with phosphorus (LGOHTWP), an industrial solid waste was adopted as adsorbent to remove Cu(II) ion from aqueous solution. Influences of experimental factors including initial pH, initial Cu(II) concentration and LGOHTWP dosage on the Cu(II) ion removal were analyzed, and the related adsorption mechanism was discussed. Aiding by Box–Behnken design based response surface methodology, an empirical quadratic equation expressing the relationship between the Cu(II) removal efficiency and adsorption parameters including initial pH, adsorbent dosage and initial Cu(II) ion concentration was obtained. In addition, the optimum conditions (initial Cu(II) concentration = 21.60 mg/L, adsorbent dosage = 79.23 g/L, initial pH = 5.71) were obtained by plotting 3-D response surfaces from the mathematical model. On the optimum conditions, the experimental Cu(II) ion removal efficiency reached 99.98%, which was in accordance with the predicted value. The results indicate that the adsorption of Cu(II) ion onto LGOHTWP is strongly dependent on pH value of the solution. Adsorption kinetics accords with the pseudo-second-order model, and the equilibrium adsorption data fits well with Langmuir isothermal model. The maximum capacity of adsorption is 26.95 mg/g at 50°C. Thermodynamic study reveals that adsorption of Cu(II) ion onto LGOHTWP is spontaneous and endothermic. In general, LGOHTWP is an efficient and promising adsorbent for Cu(II) ion removal from wastewater.

Keywords: Low grade oolitic hematite tailing with phosphorus (LGOHTWP); Cu(II) ion removal;· Adsorption; Kinetics; Thermodynamic; Response surface methodology

1. Introduction

Nowadays, due to the rapid development of metal smelting, mining, alloys formation, biocide and pigments industries, a large number of the emission containing heavy metals (Cu, Pb, Cr, Ni, Cd, As, etc.) were discharged into environments, and water pollution by heavy metals has become a serious environmental problem [1–3]. Among these heavy metals, copper(II) is a kind of toxic pollutant which do great harm to human health. Cu is easily accumulated in the food chain, which results in public health risk [4]. Poisoning with Cu in drinking water may lead to the headache, cirrhosis, heart beats, chronic anaemia, kidney damage and intestinal problems or even death, etc. [5–9]. Presently, the removal of Cu(II) ion from wastewater is regarded as an essential and urgent mission.

So far, there are various methods for metal ions removal from wastewater, such as ion exchange, reverse osmosis, chemical precipitation, membrane filtration, adsorption, etc. [10,11]. Among these mentioned methods, adsorption is

---

* Corresponding authors.

recognized as an efficient and technically convenient technique of wastewater treatment. Activated carbon is an efficient adsorbent to remove Cu(II) ions from wastewater, but its application in the industry is confined due to the high cost [12,13]. Hence, more and more attention has been paid to develop highly efficient and low-cost adsorbents, such as montmorillonite-illite type of clay [14], peat [15], zeolite [16], Palygorskitecc [17], limestone [18], natural HAP [19] and other materials [20,21]. The advantages of using these adsorbent for Cu(II) ion wastewater removal include low cost, a high removal rate, environmental friendliness and easy accessibility.

Low grade oolitic hematite tailing with phosphorus (LGOHTWP) is a kind of solid waste produced during the mining of iron ore with high phosphorus, which causes a series of problems including landslide, dust pollution and occupying land resources. Therefore, the treatment and recycling of LGOHTWP are of great urgency. Our recent work indicates that LGOHTWP possess a high Cu(II) and Cd(II) ion adsorption capacity [22,23]. However, the related adsorption mechanism is still not clear, besides, the Cu(II) ion adsorption isotherm, thermodynamics and kinetics also need further exploration.

In this work, LGOHTWP was employed as an adsorbent to remove Cu(II) ion from aqueous solution. Aiming to economically and efficiently remove Cu(II) ion from wastewater by LGOHTWP, the present work focuses on clarifying the Cu(II) adsorption behavior and optimizing the adsorption conditions. It is well known that response surface methodology (RSM) is an effective statistical method for the optimization of experimental conditions [24–26]. Thus, the method of Box–Behnken design (BBD) under RSM was introduced to explore the optimum conditions to the adsorption of Cu(II) ions by LGOHTWP in present work. The interactions of the principal adsorption process parameters including initial pH, adsorbent dosage and initial Cu(II) ion concentration were investigated using BBD-RSM. Also, the Cu(II) ion adsorption isotherm, kinetics and thermodynamics on LGOHTWP were investigated.

2. Materials and methods

2.1. Materials

LGOHTWP powder (Collected from Wushan, Chongqing) sieved through a 150 mesh was used as adsorbent in present work. The chemical composition of LGOHTWP was determined by X-ray fluorescence (XRF) (XRF-1800, Shimadzu, Japan) as listed in Table 1, the main components of LGOHTWP include Fe_2O_3, SiO_2, CaO, MgO, Al_2O_3 and P.

2.2. Procedure of adsorption experiments

First, the aqueous solutions with desired Cu(II) ion concentrations were prepared by diluting certain volumes of Cu(II) ion stock solution of 1,000 mg/L with deionized water in 150 mL glass round-bottom flasks. Here the Cu(II) stock ion solution was obtained by dissolving a defined amount of chemically pure $CuSO_4{\cdot}5H_2O$ in deionized water. The pH values of the aqueous solutions were adjusted to the designed values by adding appropriate volumes of 0.1 mol/L HCl or 0.1 mol/L NaOH. Then mixtures with different LGOHTWP dosages were obtained by adding defined amounts of adsorbent to the flasks. To ensure the homogeneous dispersion of LGOHTWP in mixtures, the mixtures were stirred for a fixed time scale with stirring speed of 265 rpm. Aqueous solution samples after different adsorption times were collected and solid was separated from liquid by filtering process, then the filtrate was used for Cu(II) ion analysis.

The relationships between response variables in adsorption experiments were studied using BBD-RSM, and the interaction effects of various variables on the removal of Cu(II) ions by LGOHTWP were explored. For statistical calculations, low, medium and high values were consecutively adopted to each of the independent variables, which were coded as 1, 0, and +1, respectively [27–29]. The complete design composed of 17 runs was implemented in triplicate to optimize the levels of selected variables. Table 2 lists the range and levels of experimental variables in present work. The variables concerned in this study include initial Cu(II) concentration (mg/L) (*A*), LGOHTWP dosage (g/L) (*B*) and initial pH (*C*), which were set at 20–60 mg/L, 20–80 g/L and 2–8, respectively. The independent parameters and the dependent output response, that is, Cu(II) ion removal efficiency (referred as $W_{Cu(II)}$ in the following) were modeled and optimized by analysis of variance (ANOVA), and then the appropriateness of the models was justified [30–33].

Cu(II) ion adsorption kinetics was evaluated at 20°C, with different initial Cu(II) ion concentrations (20–60 mg/L)

Table 1
Multielement chemical composition of LGOHTWP

Ingredient	Content (wt.%)
Fe_2O_3	36.33
SiO_2	16.73
CaO	18.19
MgO	9.12
Al_2O_3	7.44
MnO	0.39
V_2O_5	0.19
K_2O	0.24
Na_2O	0.09
P	1.37
F	0.31
S	0.05
Others	9.55

Table 2
Experimental independent variables

Variables	Factor	Range and level		
		–1	0	1
Initial Cu(II) concentration (mg/L)	*A*	20	40	60
LGOHTWP dosage (g/L)	*B*	20	50	80
Initial pH	*C*	2	5	8

as well as various adsorption times (5, 15, 25, 35 and 45 min), fixing the initial pH and LGOHTWP dosage to 5.47 and 20 g/L, respectively. Cu(II) ion adsorption isotherms were investigated at 20°C–50°C for 30 min, setting the LGOHTWP dosage, pH value and the initial Cu(II) ion concentration as 20 g/L, 5.47 and 20–60 mg/L, respectively.

The removal efficiency (W) and removal capacity of Cu(II) (q_e) are calculated as follows:

$$W(\%) = \frac{C_o - C_e}{C_o} \times 100 \tag{1}$$

$$q_e = \frac{(C_o - C_e)V}{m} \tag{2}$$

where C_o and C_e are the initial and equilibrium concentrations of Cu(II) (mg/L), respectively. V is the volume of Cu(II) aqueous solution (L), m is the mass of the adsorbent (g).

2.3. Characterization methods

To follow the removal of Cu(II) ion by LGOHTWP, a flame atomic absorption spectrophotometer (TAS-986, Persee, China) was used to analyses the Cu(II) ion concentrations of aqueous solutions after adsorption process. A Fourier-transform infrared spectrophotometer (FTIR) (Nicolet Co., USA) was adopted to collect the FTIR spectra of LGOHTWP before and after adsorption, using the transmission model (2 mg sample/100 mg spectral grade KBr) at room temperature. The particle-size distribution and specific surface area of LGOHTWP were examined by a laser diffraction particle size analyzer (LDPSA) (MS 2000, Malvern, USA) using nitrogen adsorption BET method. Microstructure of LGOHTWP was characterized by scanning electron microscopy (SEM) (JSM-7800F, JEOL, Japan). Phase composition of LGOHTWP was determined by X-ray diffraction (XRD) (D/max 2500 PC, Rigaku, Japan) with Cu Ka radiation.

3. Results and discussion

3.1. Characteristics of LGOHTWP

Fig. 1 presents the XRD pattern of LGOHTWP. Obviously, the main crystalline phases of LGOHTWP include Fe_2O_3, $CaMg(CO_3)_2$ and SiO_2. In addition, LGOHTWP contains minor amounts of rodolicoite ($FePO_4$) and fluorapatite ($Ca_5(PO_4)_3F$). Fig. 2 shows the SEM morphology of LGOHTWP powders after crushing and screening processes. It is obvious that the LGOHTWP shows a porous structure. In general, the morphology of LGOHTWP is very similar to that of oolitic hematite tailing we previously used to remove Cd(II) ions from aqueous solution [23]. The results of BET analysis indicate that the average particle size and specific surface area of LGOHTWP powder are 49.01 μm and 0.658 m^2/g, respectively. The specific surface area of LGOHTWP in present paper is smaller than that of other solid wasted adsorbents used for Cu(II) ion removal in previous paper [34,35]. The particle-size distribution of LGOHTWP is provided in Fig. 3. Obviously, the particle size of LGOHTWP distributed in a broad range, fractions of powders with size of 1–100 μm and >100 μm are 88.28 and 11.72 vol.%, respectively.

3.2. Analysis of experimental design

Table 3 presents the experimental conditions designed by Design-Expert 8.0 software based on BBD. The corresponding Cu(II) ion removal efficiencies obtained in these different experimental conditions were in the range between 60.78% and 99.45%, as listed in Table 3. According to the

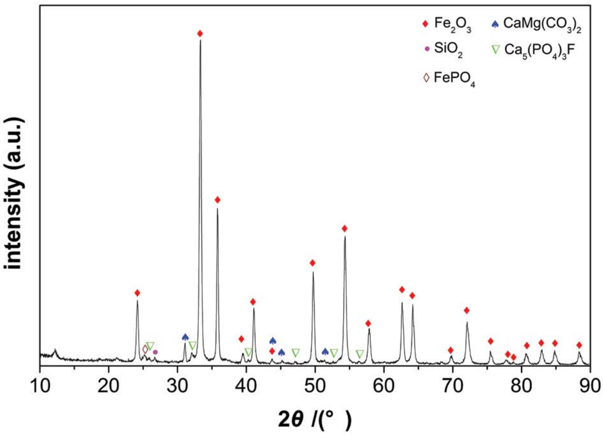

Fig. 1. XRD pattern of LGOHTWP.

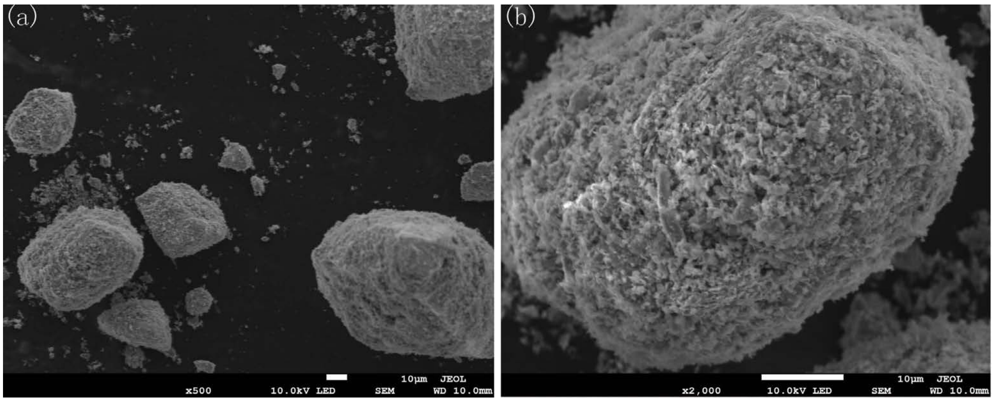

Fig. 2. SEM micrographs of LGOHTWP at different magnifications (a) 500×′ and (b) 20,000×′.

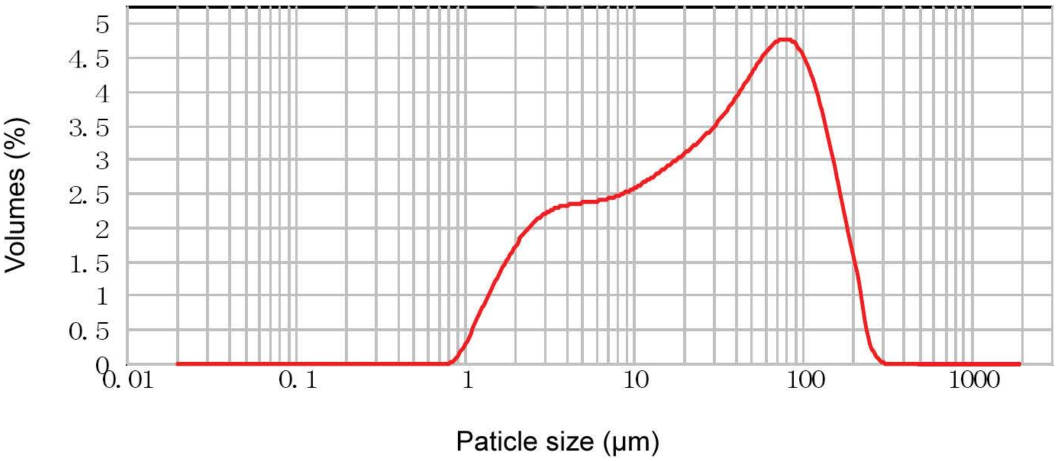

Fig. 3. Particle-size distribution of LGOHTWP.

Table 3
Experimental conditions and results of Cu(II) adsorption

Std.	Run	Factor 1:	Factor 2:	Factor 3:	Response 1:
		Initial Cu(II) concentration (mg/L)/*A*	LGOHTWP dosage (g/L)/*B*	Initial pH/*C*	Cu(II) ion removal efficiency/*M*
15	1	40	50	5	92.86
12	2	40	80	2	76.26
11	3	40	20	2	60.78
14	4	40	50	5	92.13
7	5	20	50	2	78.23
5	6	20	50	8	90.64
2	7	60	20	5	77.88
17	8	40	50	5	92.06
4	9	60	80	5	90.85
16	10	40	50	5	92.15
13	11	20	50	5	98.75
6	12	60	50	8	84.77
8	13	60	50	2	62.66
3	14	20	80	5	99.45
10	15	40	80	8	90.33
1	16	20	20	5	90.88
9	17	40	20	8	81.99

above results, an empirical quadratic equation expressing the relationship between the response and independent variables was obtained as follow:

$$
\begin{aligned}
M = {} & 92.28 - 5.50A + 5.67B + 8.73C \\
& + 1.10AB + 2.43AC - 1.79BC \\
& - 2.26B^2 - 12.95C^2
\end{aligned}
\tag{3}
$$

Table 4 lists the results of ANOVA analysis for the BBD. The suggested quadratic model [Eq. (3)] exhibits high *F*-value (572.6) and SS value (2002), while a very low *p*-value (<0.0001), which indicates that this model is valid and can well describe the correlation between $W_{\text{Cu(II)}}$ and parameters. In addition, the results in Table 4 indicate that the most important operating parameters include *A*, *B*, *C* and C^2. Table 5 shows the values of R^2 and Adj-R^2 coefficients are 0.9986 and 0.9969, respectively, which are nearly equal to 1. Fig. 4 presents the plot of the predicted values obtained by Eq. (3) vs. actual experimental results. Obviously, the predicted values coincide with the experimental results very well, which further supports the validity of the suggested quadratic model. Fig. 5 shows the perturbation plots which present the quadratic influence of *C* and nearly linear influence of *A* and *B*. The response, $W_{\text{Cu(II)}}$ was very sensitive to the initial pH (*C*). Also, with increasing the adsorbent dosage (*B*), the Cu(II) removal efficiency increases sharply at first and then increases gradually. Furthermore, the

Table 4
ANOVA table for Cu(II) adsorption with LGOHTWP

Source	Sum of squares (SS)	df	Mean square	*F*-value	*p*-value	
Model	2,002	9	222.44	572.6	<0.0001	Significant
A	267.52	1	267.52	688.64	<0.0001	
B	257.19	1	257.19	662.04	<0.0001	
C	609	1	609	1,567.66	<0.0001	
AB	4.84	1	4.84	12.46	0.0096	
AC	23.52	1	23.52	60.55	0.0001	
BC	12.74	1	12.74	32.81	0.0007	
A^2	0.3	1	0.3	0.77	0.4107	
B^2	21.57	1	21.57	55.52	0.0001	
C^2	703.69	1	703.69	1,811.39	<0.0001	
Residual	2.72	7	0.39			
Lack of fit	2.3	4	0.57	4.08	0.1389	Not significant
Pure error	0.42	3	0.14			
Cor. total	2,004.71	16				

Table 5
Model summary statistic

R^2	0.9986	Adjust R^2 (Adj-R^2)	0.9969
Adeq. precision	81.492	Standard deviation (SD)	0.62
Mean	84.45	Coefficient of variance (C.V.%)	0.73

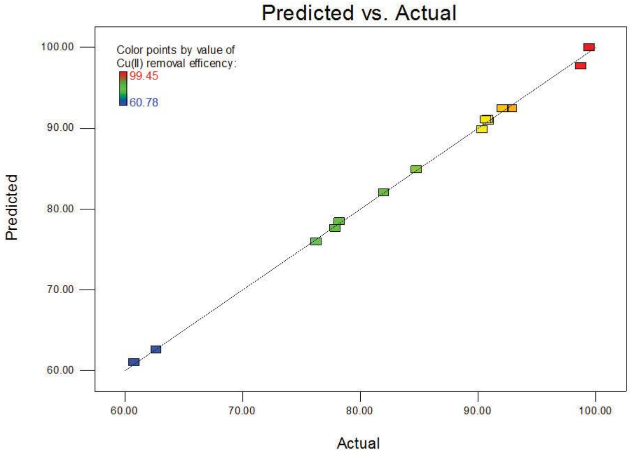

Fig. 4. Predicted vs. experimental values plot for Cu(II) adsorption using LGOHTWP (Predicted values were obtained by Eq. (3)).

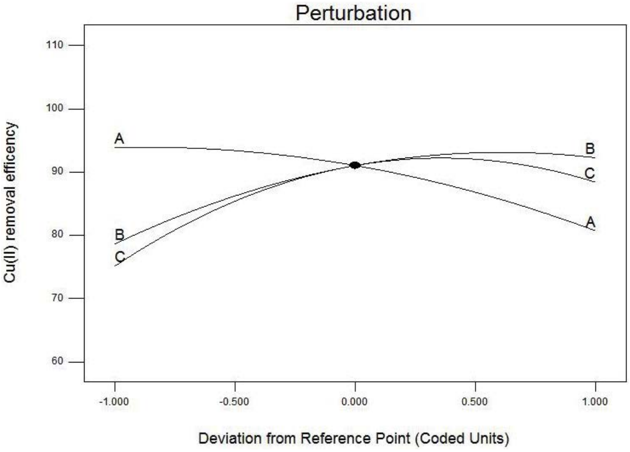

Fig. 5. Perturbation plot for Cu(II) adsorption at central points of design parameters. (A: Initial Cu(II) concentration; B: absorbent dosage; C: initial pH).

Cu(II) removal efficiency nearly linearly decreases with the initial Cu(II) concentration (*A*).

To explore the interaction effects of parameters including initial pH, adsorbent dosage and initial concentration of Cu(II) ion on the Cu(II) removal efficiency, the three-dimensional (3D) curves are plotted as shown in Figs. 6a,b–8a,b. Fig. 6a,b present the 3D surface response and contour plots for $W_{Cu(II)}$ as functions of adsorbent dosage and initial pH. The direct relevance between $W_{Cu(II)}$ and LGOHTWP dosage was observed. Obviously, increasing LGOHTWP dosage raises the reactive sites to reduce the Cu(II) ions [33,36], which leads to the increase of $W_{Cu(II)}$. In addition, it can be seen that $W_{Cu(II)}$ was high and almost steady in the wide range of pH (about 4–8) when LGOHTWP dosage was 80 g/L.

The pH value significantly influences the Cu(II) ion adsorption ability due to the fact that pH determines the species of Cu(II) ion as well as hydrolysis products on LGOHTWP surface. It is well known that the existing forms of Cu(II) vary with pH in the aqueous solution [22]. With the pH increasing, the main form of Cu(II) transforms as the following sequence: Cu^{2+}, $Cu(OH)^{+}$ and $Cu(OH)_2$. When pH is low, the dominant species of Cu(II) is Cu^{2+} [36], meanwhile, the combination of adsorbent with hydronium ions is promoted by the high concentration of H^{+}. The protonation of adsorbent gives rise to the rejection of Cu^{2+}, therefore, adsorption of Cu(II) ions onto the adsorbent is restrained [37]. With the pH increasing, more active sites were occupied, and H^+ ions were less available. Then, more Cu(II) ions can approach adsorption sites, and the hydroxy complexes absorption will be favored. Thereby, the improved adsorption capability could be attained. Whereas, the main form of Cu(II) would be $Cu(OH)_2$ in alkaline condition as the pH escalating above 7.0, which is unfavorable to the Cu(II) removal.

Fig. 7a and b depict the interactive effect of initial pH and initial Cu(II) concentration on $W_{Cu(II)}$. Obviously, the increase of initial Cu(II) concentration causes a decline in $W_{Cu(II)}$. When the initial Cu(II) concentration is high, $W_{Cu(II)}$ exhibits relatively low values, which is possibly attributed to the saturation of surface active sites with the adsorbate molecules [38]. Similar results have been observed by Davarnejad et al. [39] and Wei et al. [37] for Cu(II) removal efficiency. Moreover, it can be seen from Fig. 7b that the initial pH at which $W_{Cu(II)}$ reaches the maximum level slightly increases as the initial Cu(II) concentration increases. This can be attributed to the fact that higher initial Cu(II) concentration causes the fraction of Cu(II) ions existed as the forms of Cu^{2+} or $Cu(OH)^+$ tend to be more at a certain pH value.

Figs. 8a and b show the combined influence of initial Cu(II) concentration and LGOHTWP dosage on $W_{Cu(II)}$. As expected, $W_{Cu(II)}$ rises with LGOHTWP dosage increasing, owing to the more reduction sites available for the Cu(II) removal. However, $W_{Cu(II)}$ is difficult to reach a high value as the initial Cu(II) concentration is relatively high, even a high LGOHTWP dosage is adopted. As is shown in Fig. 8b, when the initial Cu(II) concentration was 60 mg/L, $W_{Cu(II)}$ was only 90.85% even though a high LGOHTWP dosage of 80 g/L was adopted, which may be due to the fact that high LGOHTWP dosage induces a bad dispersity of LGOHTWP particles in aqueous solution.

The BBD was employed to acquire the optimum conditions for achieving the maximum degree of Cu(II) removal efficiency. Fig. 9 shows that the basis of desirability function was equal to 1.0, the maximum $W_{Cu(II)}$ could achieve 100%,

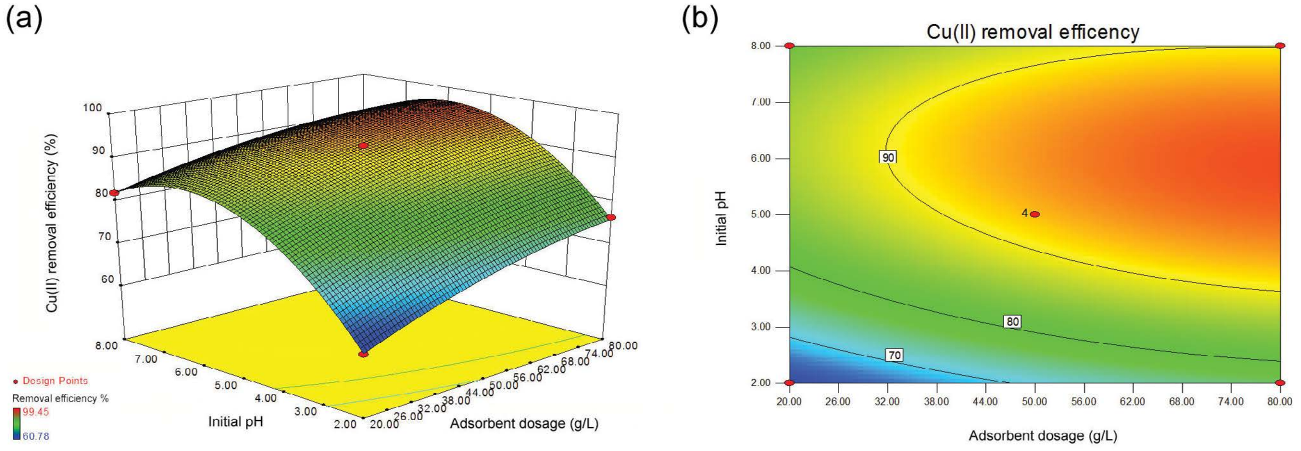

Fig. 6. (a) The response surface and (b) the contour plots of Cu(II) removal efficiency (%) as a function of adsorbent dosage and initial pH, fixing initial Cu(II) concentration to 40 mg/L.

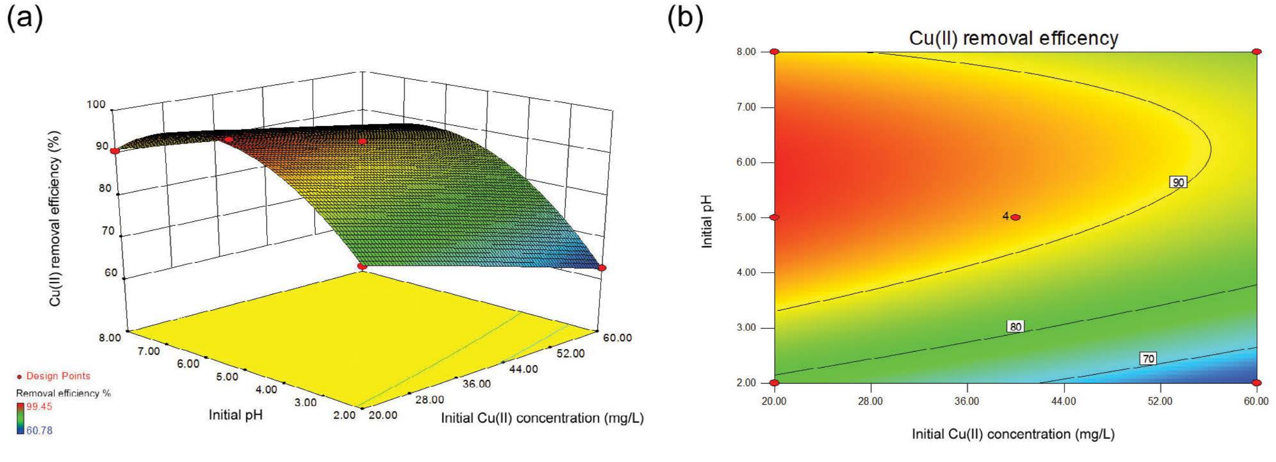

Fig. 7. (a) The response surface and (b) the contour plots of Cu(II) removal efficiency (%) as a function of initial Cu(II) concentration and initial pH, fixing adsorbent dosage to 50 g/L.

and the optimum conditions were obtained as follows: A (initial Cu(II) concentration) = 21.60 mg/L, B (adsorbent dosage) = 79.23 g/L, and C (initial pH) = 5.71. The verified experiment was performed on the suggested optimized conditions, the experimental Cu(II) removal efficiency reached 99.98%, the experimental value was generally in accordance with the above predicted value, which indicates the validity of using BBD to optimize the operating parameters of Cu(II) adsorption experiment.

3.3. Adsorption kinetics

Four kinetics models including Elovich, pseudo-first-order, intraparticle diffusion and pseudo-second-order models were adopted to assess the Cu(II) ion adsorption kinetics performance, and the potential step controlling the adsorption rate of Cu(II) ion was clarified. The four kinetics models were described by the following Eqs. (4)–(8), respectively [40–42]:

Elovich model: $q_t = \frac{1}{\beta}\ln(\alpha\beta) + \frac{1}{\beta}\ln t$ (4)

Pseudo-first-order model: $q_t = q_e\left(1 - e^{-k_1 t}\right)$ (5)

The linear equation of Eq. (5) is:

$$\ln\left(q_e - q_t\right) = \ln q_e - k_1 t \tag{6}$$

Intraparticle diffusion model: $q_t = c + k_m t^{1/2}$ (7)

Pseudo-second-order model: $\frac{t}{q_t} = \frac{1}{k_2 q_e^2} + \frac{t}{q_e}$ (8)

where q_t (mg/g) is the adsorption capacity at a certain adsorption time t (min), q_e (mg/g) is the adsorption capacity at equilibrium; α is the initial adsorption rate constant (mg/(g min)), β (g/mg) is a parameter correlated with the surface coverage degree and activation energy for chemisorption; k_1 (min^{-1}), k_m (mg/(g min$^{0.5}$)) and k_2 (g/(mg min)) are the rate constants of pseudo-first-order, intraparticle diffusion and pseudo-second-order models, respectively; c is the intercept obtained from the intraparticle diffusion model.

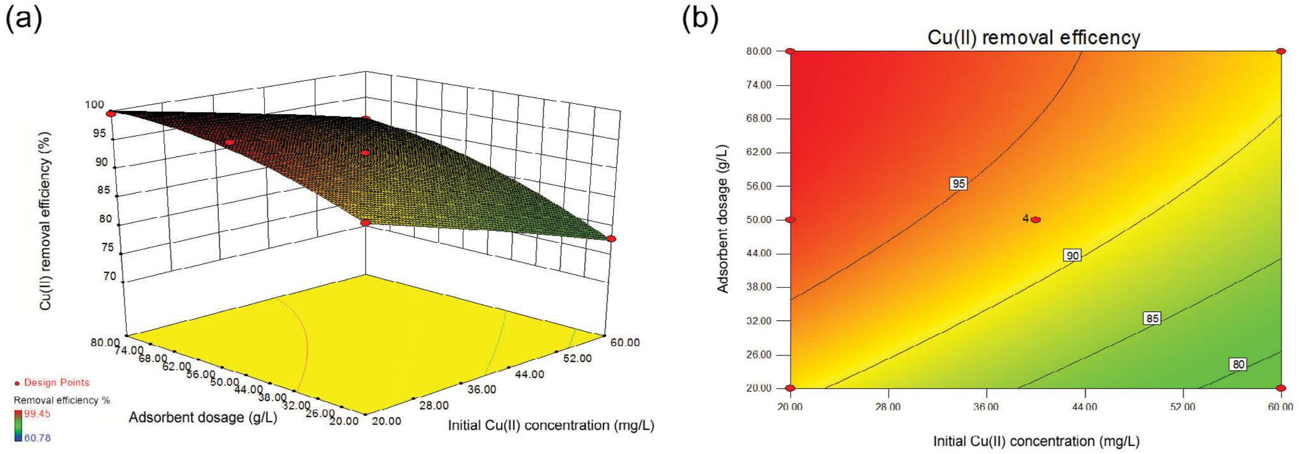

Fig. 8. (a) The response surface and (b) the contour plots of Cu(II) removal efficiency (%) as a function of initial Cu(II) concentration and adsorption dosage, fixing initial pH to 5.00.

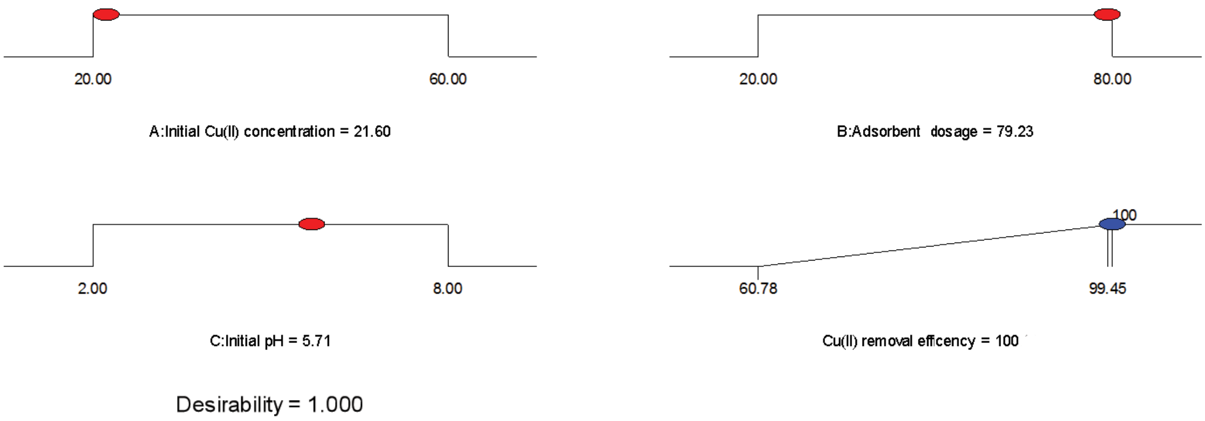

Fig. 9. Desirability function for Cu(II) adsorption by LGOHTWP.

Fig. 10 shows the plots of Cu(II) ion adsorption capacity vs. adsorption time at various initial Cu(II) ion concentrations. Initially, the adsorption is rapid and the removal efficiency over 99% is recorded within 5 min, whereas the adsorption capacity increases slowly with reaction time further prolonging. The ample adsorption sites and high Cu(II) ion concentration gradient may account for the observed rapid adsorption during incipient stage. With the reaction further progressing, the availability of adsorption sites and the Cu(II) ion concentration are reduced, thus Cu(II) ion adsorption rate decreased.

To determine the mechanisms of Cu(II) ion adsorption process, the experimental results were fitted using the linearized equations of Elovich model, pseudo-first-order model, intraparticle diffusion model and pseudo-second-order model kinetic models as shown in Fig. 11a–d. Table 6 gives the correlation coefficient (R^2) and the corresponding adsorption rate constants of the four models. Compared with the other three models, the pseudo-second-order model best describes the adsorption data. As shown in Table 6, all the correlation coefficients (R^2) of pseudo-second-order model are more than 0.99, which are higher

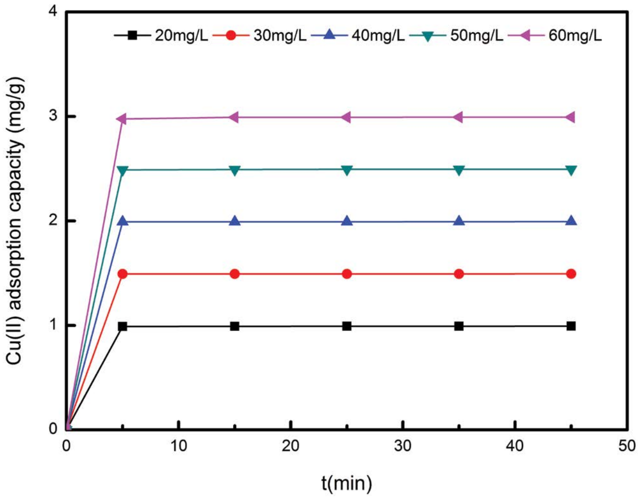

Fig. 10. The variation of adsorption capacity of LGOHTWP with adsorption time at various initial Cu(II) ion concentrations, where the initial pH, LGOHTWP dosage, and adsorption temperature were fixed to 5.47, 20 g/L and 20°C, respectively.

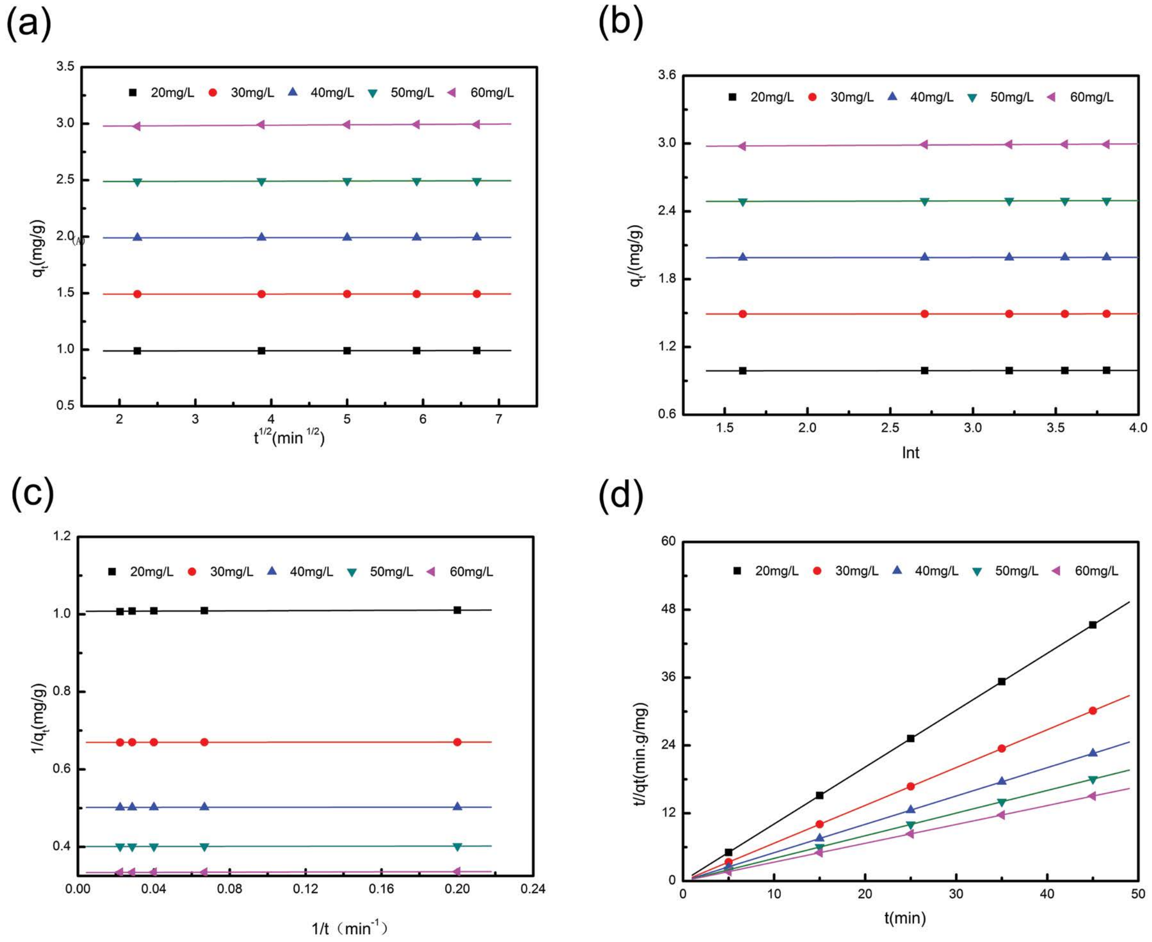

Fig. 11. Linearized form plots of different kinetic models for Cu(II) ion adsorption on LGOHTWP. (a) Intraparticle diffusion model, (b) Elovich model, (c) pseudo-first-order model and (d) pseudo-second-order model; the adsorption experiments were carried out with fixing the initial pH, LGOHTWP dosage, and adsorption temperature to 5.47, 20 g/L and 20°C, respectively.

Table 6
Estimated kinetic model parameters for Cu(II) ion adsorption on LGOHTWP

Intraparticle diffusion model: $q_t = c + k_m t^{1/2}$

Initial Cu(II) ion concentration (mg/L)	c	k_m (mg/(g min$^{0.5}$))	R^2
20	0.9877	0.0007	0.9468
30	1.4912	0.0003	0.9005
40	1.9891	0.0006	0.8700
50	2.4862	0.0012	0.8430
60	2.9723	0.0035	0.7311

Elovich model: $q_t = \frac{1}{\beta}\ln(\alpha\beta) + \frac{1}{\beta}\ln t$

Initial Cu(II) ion concentration (mg/L)	α (mg/(g min))	β (g/mg)	R^2
20	0.0014	704.23	0.8797
30	0.0006	1,556.55	0.8331
40	0.0011	900.90	0.7667
50	0.0027	366.30	0.9372
60	0.0077	130.04	0.8519

Pseudo-first-order model: $q_t = q_e\left(1 - e^{-k_1 t}\right)$

Initial Cu(II) ion concentration (mg/L)	k_1 (min^{-1})	q_e (mg/g)	R^2
20	0.0151	0.9923	0.6999
30	0.0045	1.4932	0.6621
40	0.0055	1.9926	0.5509
50	0.0132	2.4946	0.9879
60	0.0327	3.0000	0.9786

Pseudo-second-order model: $\frac{t}{q_t} = \frac{1}{k_2 q_e^2} + \frac{t}{q_e}$

Initial Cu(II) ion concentration (mg/L)	k_2 (g/(mg min))	q_e (mg/g)	R^2
20	27.43	0.9943	0.9982
30	58.70	1.4937	0.9996
40	30.87	1.9937	0.9997
50	30.26	2.4946	0.9987
60	12.61	2.9850	0.9991

than those of the above other three models. The result of Cu(II) ion adsorption kinetics suggests the process of Cu(II) ion uptake is belong to chemisorption, which indicates that the chemical adsorption reaction is the rate-limiting step [43], and the adsorption capacity is dependent on the amount of surface functional groups, active sites and bonding energy [37,44,45]. Similar results have been obtained in the Cu(II) ion removal on mesoporous dawsonite [46], 2,3-dialdehyde nano-fibrillated celluloses [47], magnetic multi-walled carbon nanotube [48], modified palygorskite [17] and EDTA-modified bentonite [49].

3.4. Isotherm adsorption

The results of adsorption isotherm experiments are shown in Fig. 12. The capacity of Cu(II) ions adsorption increases substantially with the temperature at the temperature range of 20°C–50°C. adsorption isotherm research can reveal the interaction and distribution of Cu(II) ions on the surface of adsorbent [50,51]. To evaluate the Cu(II) ions adsorption capacity of LGOHTWP, the Langmuir and Freundlich models were applied to fit the data of Fig. 12. The fitting results were compared to determine the suitable model to describe the adsorption isotherm. The linear equations of Langmuir and Freundlich models are expressed in Eqs. (9) and (10), respectively [52,53]:

$$\frac{C_e}{q_e} = \frac{1}{bq_{\max}} + \frac{C_e}{q_{\max}} \tag{9}$$

$$\log q_e = \log k + \frac{\log q_e}{n} \tag{10}$$

where c_e (mg/L) is the adsorption equilibrium concentration of Cu(II) ion, q_e (mg/g) is the Cu(II) ion adsorption capacity at equilibrium, and q_{max} (mg/g) is the maximum Cu(II) ion adsorption capacity; b (L/mg) and n are Langmuir and Freundlich constants related to the energy of adsorption, respectively; k ($mg^{1-1/n}$ $L^{1/n}$/g) is the Freundlich constant of adsorption capacity.

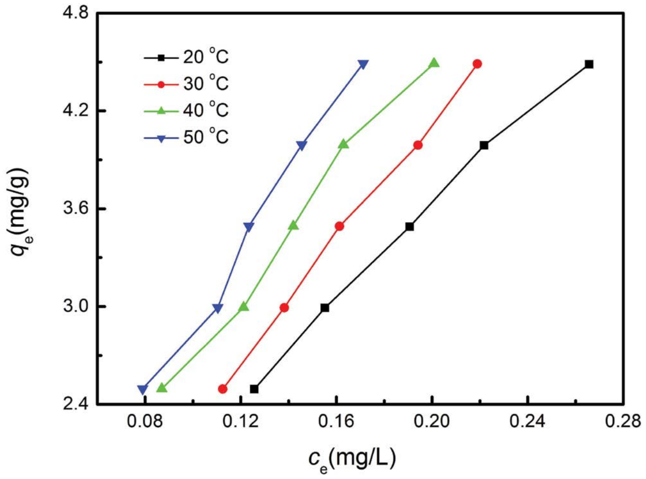

Fig. 12. Adsorption temperature of Cu(II) ion removal by LGOHTWP at different temperatures.

Fig. 13a and b show the fitted plots of adsorption isotherms using Langmuir and Freundlich models, respectively. The isotherm constants and correlation coefficient value (R^2) are listed in Table 7. Obviously, compared to the Freundlich plots, Langmuir plots fitted much better with the experimental data. High R^2 values of Langmuir plots imply that the Cu(II) ion isothermal adsorption on the LGOHTWP obeys Langmuir model. The tendency also suggests that the monomolecular adsorption may be the main adsorption mechanism of LGOHTWP.

By comparing the Cu(II) ion adsorption performance of LGOHTWP and other reported low-budget adsorbents, it can be conclude that LGOHTWP is one of the most promising materials to remove Cu(II) ion from wastewater. Table 8 lists the Cu(II) ion adsorption capacities of different adsorbents. The maximum adsorption capacity of LGOHTWP is 26.95 mg/g in this study, this is about 15.35, 8.24, 2.22 and 1.57 times of the Cu(II) ion adsorption capacities of bornean oil palm [54], spider silk [55], bentonite [56] and activated biochar [57], respectively.

3.5. Thermodynamic analysis

To quantitatively evaluate the influence of adsorption temperature on Cu(II) ion adsorption by LGOHTWP,

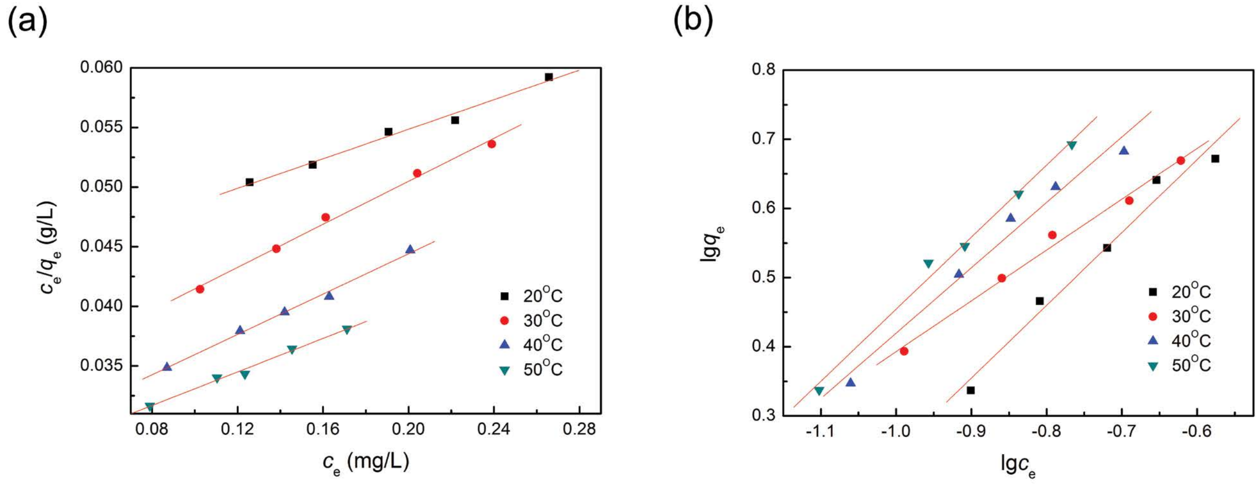

Fig. 13. Linearized form plots of isotherm for Cu(II) ion adsorption on LGOHTWP: (a) Langmuir isotherm and (b) Freundlich isotherm, where the initial pH, LGOHTWP dosage, and adsorption time were fixed to 5.47, 20 g/L and 45 min, respectively, and the initial Cu(II) ion concentration varied from 20 to 60 mg/L.

Table 7
Langmuir and Freundlich isotherm parameters for Cu(II) ion adsorption on LGOHTWP

	Langmuir isotherm: $\frac{C_e}{q_e}=\frac{1}{bq_{max}}+\frac{C_e}{q_{max}}$			Freundlich isotherm:$\log q_e=\log k+\frac{\log q_e}{n}$		
Temperature/°C	b (L/mg)	q_{max} (mg/g)	R^2	k ($mg^{1-1/n}$ $L^{1/n}$/g)	$1/n$	R^2
20	1.1082	12.98	0.9863	12.9223	1.2669	0.9747
30	1.4610	16.12	0.9944	16.9251	1.1436	0.9909
40	2.1687	16.45	0.9940	17.7877	1.2772	0.9792
50	2.6278	26.95	0.9908	17.8119	1.3326	0.9809

thermodynamic parameters including $\Delta G°$, $\Delta H°$ and $\Delta S°$ were estimated using Eqs. (11) and (12) [60].

$$\Delta G° = -RT\ln K \tag{11}$$

$$\Delta G° = \Delta H° - T\Delta S° \tag{12}$$

where $\Delta G°$ is standard free energy change, R is the gas constant, T (K) is the temperature, and the equilibrium constant K is converted by the Langmuir constant b (L/mol) [61], $\Delta H°$ and $\Delta S°$ are standard enthalpy change and standard entropy change, respectively.

Table 9 shows the thermodynamic parameters of Cu(II) ion adsorption. The $\Delta G°$ values are negative, indicating that LGOHTWP adsorbent possess spontaneous and thermodynamically favorable adsorption nature. In addition, the $\Delta G°$ values decreases when the temperature increases, which implies that higher temperature favors Cu(II) ion removal by LGOHTWP. The $\Delta S°$ and $\Delta H°$ values are acquired from the slope and intercept of $\Delta G°$ against T (Fig. 14). The $\Delta H°$ value of 23.47 kJ/mol indicates the endothermic nature of Cu(II) ion adsorption onto LGOHTWP at 20°C–50°C. Moreover, the $\Delta S°$ value of 80.92 J/(mol K) suggests that the randomness at the adsorbent-solution interface increases after Cu(II) ion adsorption, which is due to the fact that the water molecules or the hydrated ions releases from water on the surface of LGOHTWP during the process of Cu(II) ion removal [62].

Table 8
Comparison of maximum of Cu(II) ion adsorption capacities of different adsorbents

No.	Material	Adsorption capacity (mg/g)	References
1	Activated carbon	19.5	[17]
2	Natural HAp	24.78	[19]
3	As-produced CNTs	8.25	[22]
4	Bentonite	12.1	[56]
5	Activated biochar	17.2	[57]
6	Spider silk	3.27	[55]
7	*Aspergillus flavus* biomass	10.82	[55]
8	Bornean oil palm	1.756	[54]
9	Wheat straw	4.42	[58]
10	Modified pine sawdust	101.6	[59]
11	LGOHTWP	26.95	This study

Table 9
Thermodynamic parameters for the adsorption of Cu(II) ion on LGOHTWP

Temperature (K)	$\Delta G°$ (J/mol)	$\Delta H°$ (kJ/mol)	$\Delta S°$ (J/(mol K))
293	–250.27	23.47	80.92
303	–955.06		
313	–2014.50		
323	–2594.51		

3.6. FTIR analysis and adsorption mechanism study

The specific surface of adsorbents highly affects the metal sorption behavior [63,64]. As mentioned above, the main compositions of LGOHTWP are hematite, dolomite and quartz. It is well known that the surfaces of oxide and dolomite in aqueous solution often coordinate with water molecules [65,66], therefore, a large amount of surface hydroxyl groups will cover the surface of LGOHTWP. The functional groups favors the Cu(II) ion adsorption onto the LGOHTWP. To clarify the adsorption mechanisms of the LGOHTWP, the FTIR spectra (Fig. 15) of LGOHTWP samples before and after adsorption were collected. The adsorption experiment was carried out at 20°C for 45 min, fixing the initial concentration of Cu(II) ion, pH and LGOHTWP to 30 mg/L, 5.47 and 20 g/L, respectively. The

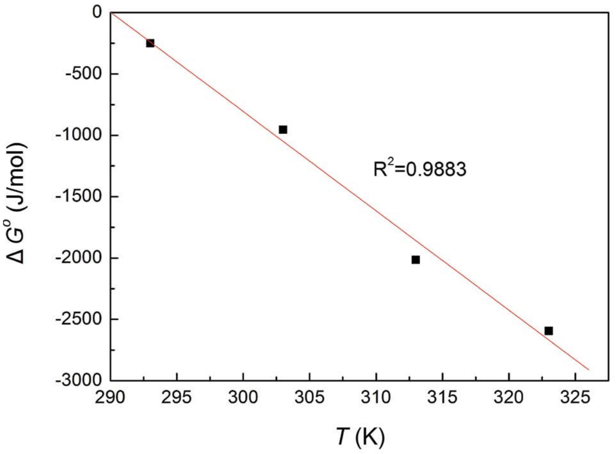

Fig. 14. Plot of $\Delta G°$ vs. T for Cu(II) ion adsorption by LGOHTWP, where the initial pH, LGOHTWP dosage, and adsorption time were fixed to 5.47, 20 g/L and 45 min, respectively, and the initial Cu(II) ion concentration varied from 20 to 60 mg/L.

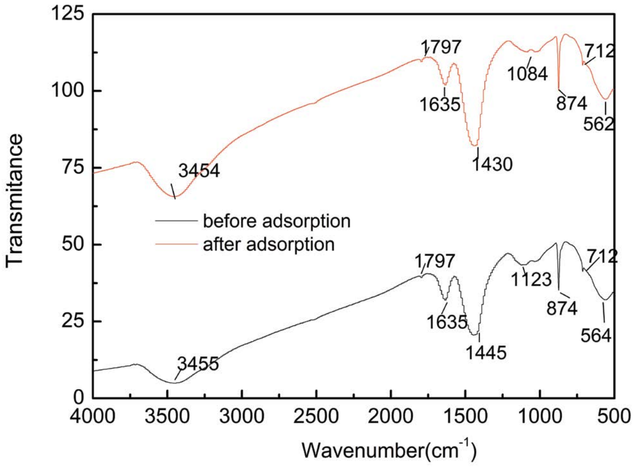

Fig. 15. FTIR spectra of LGOHTWP samples before and after Cu(II) ion adsorption, the adsorption experiments were carried out at 20°C, and the pH value, the initial Cu(II) ion concentration, LGOHTWP dosage, and adsorption time were fixed to 5.47, 30 mg/L, 20 g/L, and 45 min, respectively.

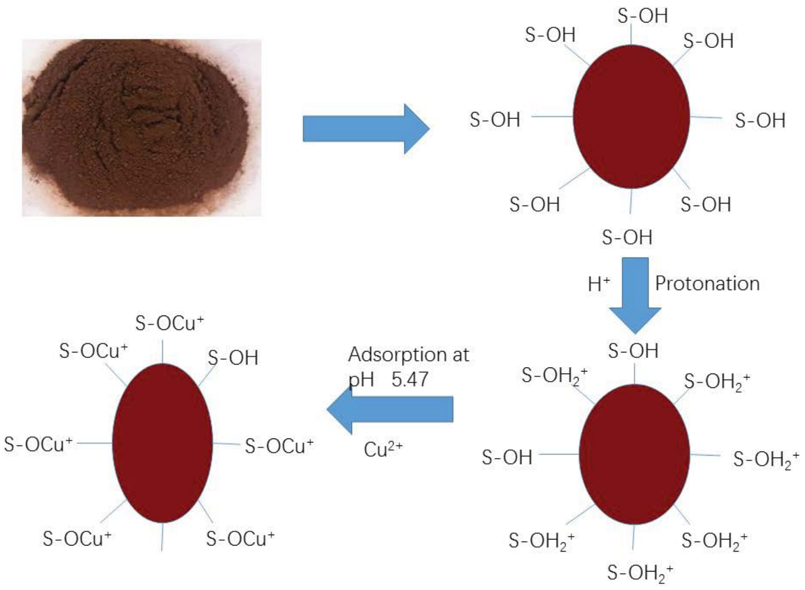

Fig. 16. Schematic diagram of the major mechanism for adsorption of Cu(II) ion onto the surface of LGOHTWP.

valleys at 3,455 and 1,635 cm^{-1} in FTIR spectrum of the sample before adsorption are due to the stretching and bending vibrations of physisorbed water molecule (H–O–H) [65,67], similar valleys (3,454 and 1,635 cm^{-1}) are observed in FTIR spectrum of the sample after adsorption. For the sample before adsorption, the stretchings of multicentered hydroxyl group (S–OH, where S is the central ion on the surface of mineral) induces the bands at 1,445, 1,123, 874 and 564 cm^{-1} [68]. After LGOHTWP reacting with Cu(II) ion solution, the S–OH bands at the two valleys of 1,445 and 1,123 cm^{-1} are completely disappeared, while two new valleys appear at 1,430 and 1,084 cm^{-1}. The new bands are mainly involved in the molecular structure of inner-sphere surface complex (S–O–Cu). This suggests that S–OH are exchanged by the Cu(II) ion. Fig. 16 illustrates the above proposed mechanism for the process of Cu(II) ion adsorption. Cu(II) ion adsorption occurs at the LGOHTWP/solution interface when pH value is relatively low. Complexation, that is, the Cu(II) ions replacing the surface hydroxyl groups is the principal mechanism of Cu(II) ion adsorption.

4. Conclusions

In this work, a simple and high-efficiency method to remove Cu(II) ion from aqueous solution by LGOHTWP has been developed. The BBD statistical design method under RSM were used to optimize conditions for the Cu(II) ion removal by LGOHTWP. The Cu(II) ion adsorption kinetics, isotherm and thermodynamic parameters were evaluated, and the adsorption mechanisms were clarified. According to the results of this research, conclusions can be drawn as follows:

- By using BBD-RSM method, the optimal conditions for Cu(II) adsorption by LGOHTWP were obtained: the adsorbent dosage was 79.23 g/L, initial pH was 5.71, and Cu(II) concentration was 21.60 mg/L. The Cu(II) ion removal efficiency could reach nearly 100% on the optimal adsorption conditions.
- Cu(II) ion in aqueous solution is adsorbed rapidly by LGOHTWP. The pseudo-second-order kinetic model can well describe the adsorption kinetics of Cu(II) ion. The process of Cu(II) ion removal is chiefly controlled by the chemisorption, which is the rate-determining step. The dominant adsorption mechanism is the replacement of the surface hydroxyl groups of LGOHTWP by the Cu(II) ions (complexation).
- Elevating adsorption temperature favors the adsorption removal of Cu(II) ion on LGOHTWP. The isotherm of Cu(II) ion adsorption onto LGOHTWP at different temperatures agrees well with Langmuir equations. LGOHTWP exhibits a maximum Cu(II) ion adsorption capacity of 26.95 mg/g at 50°C.
- Thermodynamic parameters results indicate that the Cu(II) ion uptake reactions by LGOHTWP is spontaneous and endothermic. The $\Delta G°$ value decreases from –250.27 to –2,594.51 J/mol as the adsorption temperature increases from 20°C to 50°C. The values of $\Delta H°$ and $\Delta S°$ are 23.47 kJ/mol and 80.92 J/(mol K), respectively.
- LGOHTWP is an excellent and high effective adsorbent in removal of Cu(II) ion from wastewater, based on its eminent Cu(II) ion adsorption performance.

Acknowledgements

This research was funded by Project Supported by the Venture & Innovation Support Program for Chongqing Overseas Returnees (Grant No. cx2020088), the Scientific and Technological Research Program of Chongqing Municipal Education Commission (Grant No. KJQN201801507 and KJQN202001534), the graduate science and technology innovation training program project of Chongqing University of Science & Technology (Grant No. YKJCX2020203), the National Training Program of Innovation and Entrepreneurship for Undergraduates (Grant No. 202111551018) and the National Natural Science Foundation of China (Grant No. 51674057, 51904052 and 52174331). This work was also financially supported by Innovation research group of universities in Chongqing(CXQT21030).

References

[1] A. Kamari, S.N.M. Yusoff, F. Abdullah, W.P. Putra, Biosorptive removal of Cu(II), Ni(II) and Pb(II) ions from aqueous solutions using coconut dregs residue: adsorption and characterisation studies, J. Environ. Chem. Eng., 2 (2014) 1912–1919.

[2] X.L. Yuan, W.T. Xia, J. An, X.J. Zhou, X.Y. Xiang, J.G. Yin, W.Q. Yang, Adsorption characteristics of Pb(II) ions onto wasted iron ore tailing with phosphorus used as natural adsorbent from aqueous solution, Desal. Water Treat., 98 (2017) 222–232.

[3] H.A. Abubshait, A.A. Farag, M.A. El-Raouf, N.A. Negm, E.A. Mohamed, Graphene oxide modified thiosemicarbazide nanocomposite as an effective eliminator for heavy metal ions, J. Mol. Liq., 327 (2021) 114790, doi: 10.1016/j.molliq.2020.114790.

[4] M. Gupta, H. Gupta, D.S. Kharat, Adsorption of Cu(II) by low cost adsorbents and the cost analysis, Environ. Technol. Innovation, 10 (2018) 91–01.

[5] L. Zhao, Q. Zhang, X.B. Li, J.J. Ye, J.Y. Chen, Adsorption of Cu(II) by phosphogypsum modified with sodium dodecyl benzene sulfonate, J. Hazard. Mater., 387 (2020) 121808, doi: 10.1016/j.jhazmat.2019.121808.

[6] S.A. Hosseini, Z. Shokri, S. Karami, Adsorption of Cu(II) to mGO@Urea and its application for the catalytic reduction of 4-NP, J. Ind. Eng. Chem., 75 (2019) 52–60.

[7] S. Dandil, D.A. Sahbaz, C. Acikgoz, Adsorption of Cu(II) ions onto crosslinked chitosan/waste active sludge char (WASC) beads: kinetic, equilibrium, and thermodynamic study, Int. J. Biol. Macromol., 136 (2019) 668–675.

[8] M. Ahmad, K. Manzoor, P. Venkatachalam, S. Ikram, Kinetic and thermodynamic evaluation of adsorption of Cu(II) by thiosemicarbazide chitosan, Int. J. Biol. Macromol., 92 (2016) 910–919.

[9] Z.L. Du, T. Zheng, P. Wang, Experimental and modelling studies on fixed bed adsorption for Cu(II) removal from aqueous solution by carboxyl modified jute fiber, Powder Technol., 338 (2018) 952–959.

[10] J.-S. Cao, C. Wang, F. Fang, J.-X. Lin, Removal of heavy metal Cu(II) in simulated aquaculture wastewater by modified palygorskite, Environ. Pollut., 219 (2016) 924–931.

[11] F. Liu, K.G. Zhou, Q.Z. Chen, A.H. Wang, W. Chen, Application of magnetic ferrite nanoparticles for removal of Cu(II) from copper-ammonia wastewater, J. Alloys Compd., 773 (2019) 140–149.

[12] H.M.H. Gad, A.A. El-Sayed, Activated carbon from agricultural by-products for the removal of Rhodamine-B from aqueous solution, J. Hazard. Mater., 168 (2009) 1070–1081.

[13] F. Di Natale, A. Erto, A. Lancia, Desorption of arsenic from exhaust activated carbons used for water purification, J. Hazard. Mater., 260 (2013) 451–458.

[14] J.U.K. Oubagaranadin, Z.V.P. Murthy, V.P. Mallapur, Removal of Cu(II) and Zn(II) from industrial wastewater by acid-activated montmorillonite-illite type of clay, C.R. Chim., 13 (2010) 1359–1363.

[15] Y.S. Ho, J.F. Porter, G. McKay, Equilibrium isotherm studies for the sorption of divalent metal ions onto peat: copper, nickel and lead single component systems, Water Air Soil Pollut., 141 (2002) 1–33.

[16] M. Akgül, A. Karabakan, Promoted dye adsorption performance over desilicated natural zeolite, Microporous Mesoporous Mater., 145 (2011) 157–164.

[17] M. Madhava Rao, D.K. Ramana, K. Seshaiah, M.C. Wang, S.W. Chang Chien, Removal of some metal ions by activated carbon prepared from *Phaseolus aureus* hulls, J. Hazard. Mater., 166 (2009) 1006–1013.

[18] X.L. Peng, W.J. Chen, Z.J. He, D. Li, H. Liu, H. Jin, G.G. Zhou, F.G. Xu, Removal of Cu(II) from wastewater using doped HAP-coated-limestone, J. Mol. Liq., 293 (2019) 111502, doi: 10.1016/j.molliq.2019.111502.

[19] O. Rosskopfová, M. Galamboš, J. Ometákov, M. Čaplovičová, P. Rajec, Study of sorption processes of copper on synthetic hydroxyapatite, J. Radioanal. Nucl. Chem., 293 (2012) 641–647.

[20] Y.-H. Chen, A.L. Fu, Kinetic study on removal of copper(II) using goethite and hematite nano-photocatalysts, J. Colloid Interface Sci., 347 (2010) 277–281.

[21] C.-H. Wu, Studies of the equilibrium and thermodynamics of the adsorption of Cu^{2+} onto as-produced and modified carbon nanotubes, J. Colloid Interface Sci., 311 (2007) 338–346.

[22] X.L. Yuan, D.S. Zhou, W.T. Xia, Q.Y. Huang, Low-Grade Phosphorus-Containing Iron Ore for the Removal of Cu(II) Ion From Wastewater, 10th International Symposium on High-Temperature Metallurgical Processing. The Minerals, Metals & Materials Series, Springer, Cham, 2019, pp. 705–712.

[23] X.L. Yuan, D.S. Zhou, W.T. Xia, J. An, X.J. Zhou, J.G. Yin. Adsorption of Cd(II) ions from aqueous solution by wasted low-grade phosphorus-containing oolitic hematite: equilibrium, kinetics, and thermodynamics, Desal. Water Treat., 192 (2020) 271–282.

[24] A. Asfaram, M. Ghaedi, M.H.A. Azqhandi, A. Goudarzi, S. Hajati, Ultrasound-assisted binary adsorption of dyes onto Mn@CuS/ZnS-NC-AC as a novel adsorbent: application of chemometrics for optimization and modeling, J. Ind. Eng. Chem., 54 (2017) 377–338.

[25] E.A. Dil, M. Ghaedi, A. Asfaram, S. Hajati, F. Mehrabi, A. Goudarzi, Preparation of nanomaterials for the ultrasound-enhanced removal of Pb^{2+} ions and malachite green dye: chemometric optimization and modeling, Ultrason. Sonochem., 34 (2017) 677–691.

[26] E.A. Dil, M. Ghaedi, G.R. Ghezelbash, A. Asfaram, Multi-responses optimization of simultaneous biosorption of cationic dyes by live yeast Yarrowia lipolytica 70562 from binary solution: application of first order derivative spectrophotometry, Ecotoxicol. Environ. Saf., 139 (2017) 158–164.

[27] F. Ansari, M. Ghaedi, M. Taghdiri, A. Asfaram, Application of ZnO nanorods loaded on activated carbon for ultrasonic assisted dyes removal: experimental design and derivative spectrophotometry method, Ultrason. Sonochem., 33 (2016) 197–209.

[28] A.R. Bagheri, M. Ghaedi, A. Asfaram, R. Jannesar, A. Goudarzi, Design and construction of nanoscale material for ultrasonic assisted adsorption of dyes: application of derivative spectrophotometry and experimental design methodology, Ultrason. Sonochem., 35 (2017) 112–113.

[29] D. Naghipour, K. Taghavi, J. Jaafari, Y. Mahdavi, M.G. Ghozikali, R. Ameri, A. Jamshidi, A.H. Mahvi, Statistical modeling and optimization of the phosphorus biosorption by modified *Lemna minor* from aqueous solution using response surface methodology (RSM), Desal. Water Treat., 57 (2016) 19431–19442.

[30] S.D. Ashrafi, H. Kamani, J. Jaafari, A.H. Mahvi, Experimental design and response surface modeling for optimization of fluoroquinolone removal from aqueous solution by NaOH-modified rice husk, Desal. Water Treat., 57 (2016) 16456–16465.

[31] M. Arabi, A. Ostovan, M. Ghaedi, M.K. Purkait, Novel strategy for synthesis of magnetic dummy molecularly imprinted nanoparticles based on functionalized silica as an efficient sorbent for the determination of acrylamide in potato chips: optimization by experimental design methodology, Talanta, 154 (2016) 526–532.

[32] E. Alipanahpour Dil, M. Ghaedi, A.M. Ghaedi, A. Asfaram, A. Goudarzi, S. Hajati, M. Soylak, S. Agarwal, V.K. Gupta, Modeling of quaternary dyes adsorption onto ZnO–NR–AC artificial neural network: analysis by derivative spectrophotometry, J. Ind. Eng. Chem., 34 (2016) 186–197.

[33] J. Jaafari, M.G. Ghozikali, A. Azari, M.B. Delkhosh, A.B. Javid, A.A. Mohammadi, S. Agarwal, V.K. Gupta, M. Sillanpää, A.G. Tkachev, A.E. Burakov, Adsorption of *p*-Cresol on Al_2O_3 coated multi-walled carbon nanotubes: response surface methodology and isotherm study, J. Ind. Eng. Chem., 57 (2018) 396–404.

[34] V.D. Chavan, V.P. Kothavale, S.C. Sahoo, P. Kollu, T.D. Dongale, P.S. Patil, P.B. Patil, Adsorption and kinetic behavior of Cu(II)

ions from aqueous solution on DMSA functionalized magnetic nanoparticles, Physica B, 571 (2014) 273–279.

[35] L. Zhao, Q. Zhang, X. Li, J. Ye, J. Chen, Adsorption of Cu(II) by phosphogypsum modified with sodium dodecyl benzene sulfonate, J. Hazard. Mater., 387 (2020) 121808, doi: 10.1016/j.jhazmat.2019.121808.

[36] F.J. Cerino-Córdova, P.E. Díaz-Flores, R.B. García-Reyes, E. Soto-Regalado, R. Gómez-González, M.T. Garza-González, E. Bustamante-Alcántara, Biosorption of Cu(II) and Pb(II) from aqueous solutions by chemically modified spent coffee grains, Int. J. Environ. Sci. Technol., 10 (2013) 611–622.

[37] W. Wei, X. Han, M. Zhang, Y. Zhang, Y. Zhang, C. Zheng, Macromolecular humic acid modified nano-hydroxyapatite for simultaneous removal of Cu(II) and methylene blue from aqueous solution: experimental design and adsorption study, Int. J. Biol. Macromol., 150 (2020) 849–860.

[38] S. Chowdhury, P. Saha, Sea shell powder as a new adsorbent to remove Basic Green 4 (Malachite Green) from aqueous solutions: equilibrium, kinetic and thermodynamic studies, J. Chem. Eng., 164 (2010) 168–177.

[39] R. Davarnejad, P. Panahi, Cu(II) removal from aqueous wastewaters by adsorption on the modified Henna with Fe_3O_4 nanoparticles using response surface methodology, Sep. Purif. Technol., 158 (2016) 286–292.

[40] Y.S. Ho, G. Mckay, Sorption of dye from aqueous solution by peat, J. Chem. Eng., 70 (1998) 115–124.

[41] Y.S. Ho, G. Mckay (Fellow), Kinetic models for the sorption of dye from aqueous solution by wood, Process Saf. Environ. Prot., 76 (1998) 183–191.

[42] D.L. Sparks, Chapter 7 – Rates of Chemical Weathering, D.L. Sparks, Ed., Kinetics of Soil Chemical Processes, Academic Press, San Diego, CA, 1989, pp. 146–162.

[43] Y. Deng, Z. Gao, B. Liu, X. Hu, Z. Wei, C. Sun, Selective removal of lead from aqueous solutions by ethylenediamine-modified attapulgite, J. Chem. Eng., 223 (2013) 91–98.

[44] S. Dawood, T.K. Sen, Removal of anionic dye Congo red from aqueous solution by raw pine and acid-treated pine cone powder as adsorbent: equilibrium, thermodynamic, kinetics, mechanism and process design, Water Res., 46 (2012) 1933–1946.

[45] Y.F. Feng, D.D. Dionysiou, Y.H. Wu, H. Zhou, L.H. Xue, S.Y. He, L.Z. Yang, Adsorption of dyestuff from aqueous solutions through oxalic acid-modified swede rape straw: adsorption process and disposal methodology of depleted bioadsorbents, Bioresour. Technol., 138 (2013) 191–197.

[46] B. Li, J.-Q. Zheng, J.-Z. Guo, C.-Q. Dai, A novel route to synthesize MOFs-derived mesoporous dawsonite and application in elimination of Cu(II) from wastewater, Chem. Eng. J., 383 (2020) 123174, doi: 10.1016/j.cej.2019.123174.

[47] Z.H. Lei, W.H. Gao, J.S. Zeng, B. Wang, J. Xu, The mechanism of Cu(II) adsorption onto 2,3-dialdehyde nano-fibrillated celluloses, Carbohydr. Polym., 230 (2020) 115631, doi: 10.1016/j.carbpol.2019.115631.

[48] W.-W. Tang, G.-M. Zeng, J.-L. Gong, Y. Liu, X.-Y. Wang, Y.-Y. Liu, Z.-F. Liu, L. Chen, X.-R. Zhang, D.-Z. Tu, Simultaneous adsorption of atrazine and Cu(II) from wastewater by magnetic multi-walled carbon nanotube, Chem. Eng. J., 211–212 (2012) 470–478.

[49] M.L.F.A. De Castro, M.L.B. Abad, D.A.G. Sumalinog, R.R.M. Abarca, P. Paoprasert, M.D.G. de Luna, Adsorption of Methylene Blue dye and Cu(II) ions on EDTA-modified bentonite: isotherm, kinetic and thermodynamic studies, Sustainable Environ. Res., 28 (2018) 197–205.

[50] H.M.F. Freundlich, Über die adsorption in lösungen, Z. Phys. Chem., 57 (1906) 385–470.

[51] I. Langmuir, The adsorption of gases on plane surfaces of glass, mica and platinum, J. Am. Chem. Soc., 40 (1918) 1361–1403.

[52] X.Y. Zhang, X.B. Jiang, X.L. Zhu, X.Z. Kong, Effective enhancement of Cu ions adsorption on porous polyurea adsorbent by carboxylic modification of its terminal amine groups, React. Funct. Polym., 147 (2020) 104450, doi: 10.1016/j.reactfunctpolym.2019.104450.

[53] S.K. Pradhan, V. Pareek, J. Panwar, S. Gupta, Synthesis and characterization of ecofriendly silver nanoparticles combined with yttrium oxide ($Ag\text{-}Y_2O_3$) nanocomposite with assorted adsorption capacity for Cu(II) and Cr(VI) removal: a mechanism perspective, J. Water Process Eng., 32 (2019) 100917, doi: 10.1016/j.jwpe.2019.100917.

[54] H.L.H. Chong, P.S. Chia, M.N. Ahmad, The adsorption of heavy metal by Bornean oil palm shell and its potential application as constructed wetland media, Bioresour. Technol., 130 (2013) 181–186.

[55] L. Pelit, F.N. Ertaş, A.E. Eroğlu, T. Shahwan, H. Tural, Biosorption of Cu(II) and Pb(II) ions from aqueous solution by natural spider silk, Bioresour. Technol., 102 (2011) 8807–8813.

[56] W.-C. Tsai, M.D.G. de Luna, H.L.P. Bermillo-Arriesgado, C.M. Futalan, J.I. Colades, M.-W. Wan, Competitive fixed-bed adsorption of Pb(II), Cu(II), and Ni(II) from aqueous solution using chitosan-coated bentonite, Int. J. Polym. Sci., 2016 (2016) 1608939, doi: 10.1155/2016/1608939.

[57] M.D.G. de Luna, E.D. Flores, M.C.B. Cenia, M.-C. Lu, Removal of copper ions from aqueous solution by adlai shell (*Coix lacryma-jobi* L.) adsorbents, Bioresour. Technol., 192 (2015) 841–844.

[58] Y. Wu, L. Zhang, C. Gao, J. Ma, X. Ma, R. Han, Adsorption of copper ions and methylene blue in a single and binary system on wheat straw, J. Chem. Eng. Data, 54 (2009) 3229–3234.

[59] R.Z. Zhang, Y.B. Zhou, X.C. Gu, J. Lu, Competitive adsorption of methylene blue and Cu^{2+} onto citric acid modified pine sawdust, CLEAN-Soil Air Water, 43 (2015) 96–103.

[60] Y. Liu, Is the free energy change of adsorption correctly calculated?, J. Chem. Eng. Data, 54 (2009) 1981–1985.

[61] A.R. Kul, H. Koyuncu, Adsorption of Cu(II) ions from aqueous solution by native and activated bentonite: kinetic, equilibrium and thermodynamic study, J. Hazard. Mater., 179 (2010) 332–339.

[62] V.K. Gupta, M.R. Ganjali, A. Nayak, B. Bhushan, S. Agarwal, Enhanced heavy metals removal and recovery by mesoporous adsorbent prepared from waste rubber tire, J. Chem. Eng., 197 (2012) 330–342.

[63] D. Alidoust, M. Kawahigashi, S. Yoshizawa, H. Sumida, M. Watanabe, Mechanism of cadmium biosorption from aqueous solutions using calcined oyster shells, J. Environ. Manage., 150 (2015) 103–110.

[64] G.F. Coelho, A.C. Gonçalves Jr., C.R.T. Tarley, J. Casarin, H. Nacke, M.A. Francziskowski, Removal of metal ions Cd(II), Pb(II), and Cr(III) from water by the cashew nut shell *Anacardium occidentale* L, Ecol. Eng., 73 (2014) 514–525.

[65] X.L. Yuan, C.G. Bai, W.T. Xia, J. An, Acid–base properties and surface complexation modeling of phosphate anion adsorption by wasted low grade iron ore with high phosphorus, J. Colloid Interface Sci., 428 (2014) 208–214.

[66] E. Pehlivan, A.M. Ozkan, S. Dinç, S. Parlayici, Adsorption of Cu^{2+} and Pb^{2+} ion on dolomite powder, J. Hazard. Mater., 167 (2009) 1044–1049.

[67] J.B. Lǚ, H.J. Liu, R.P. Liu, X. Zhao, L.P. Sun, H. Qu, Adsorptive removal of phosphate by a nanostructured Fe–Al–Mn trimetal oxide adsorbent, Powder Technol., 233 (2013) 146–154.

[68] K. Karageorgiou, M. Paschalis, G.N. Anastassakis, Removal of phosphate species from solution by adsorption onto calcite used as natural adsorbent, J. Hazard. Mater., 139 (2007) 447–452.